Magnetic sensor sensitivity map: application to low field NMR gradiometer

Nazim Lechea[1,2], Thierry Ditchi[2], Céline Filloy[2], Stéphane Holé[2,*], Jérôme Lesueur[2] and Jérôme Lucas[1]

[1] *Electrical Engineering Laboratory (LEG), ESPCI-ParisTech, 10 rue Vauquelin, 75005 Paris, France*
[2] *Physics and Material Study Laboratory (LPEM), UPMC, ESPCI-ParisTech, CNRS 8213, 10 rue Vauquelin, 75005 Paris, France*
** Corresponding author:* nazim.lechea@espci.fr

KEYWORDS: Magnetic sensor, Sensitivity map, Gradiometer, Pick-up coil, Nuclear Magnetic Resonance, Magnetic Resonance Imaging, Low Field, Eddy current.

In this paper we calculate the analytical expression of magnetic induction sensor sensitivity map. That expression can be used for any kind of magnetic induction sensors and can help to save time in the design and development. It is applied here to the study of low field nuclear magnetic resonance (NMR) gradiometers. Gradiometers consists of pick-up coil specially designed to reduce the influence of far magnetic sources while keeping sufficient sensitivity for near sources. In this paper, the sensibility maps of various kinds of gradiometers are studied.

Manuscript received: January XX, 2011 / Accepted: January 10, 2011

NOMENCLATURE

$\vec{E}$: electric field
$\vec{B}, \vec{H}$: induction and magnetic field
μ_0: vacuum magnetic permeability
$\vec{A}, \delta\vec{A}$: magnetic potential vector and its variation.
$\mu, \delta\mu$: material magnetic permeability and variation
$\sigma, \delta\sigma$: material conductivity and its variation
$\vec{J}, \delta\vec{J}$: current density and its variation
$\vec{J}_s, \delta\vec{J}_s$: current density sources and its variation
$\vec{M}, \delta\vec{M}$: permanent magnetization and its variation
$\varphi, \delta\varphi$: total magnetic flux and its variation
$\varphi_s, \delta\varphi_s$: magnetic flux sources and its variation
φ_m: measured flux
$\Delta\varphi$: flux variation
L, L_{mj} : inductance and inductance tensor
$i, \delta i$: electric current and its variation.
v: voltage
S: sensor sensitivity, p: physical parameter
$\mathcal{C}_m, \mathcal{L}_m, \mathcal{S}_m$: measuring circuit, path, and cross section
$\vec{\beta}_m, \vec{\alpha}_m$: induction field and potential induced by 1A in $\mathcal{C}_m$
A, B: equilibrium states
r: radius, b: gradiometer baseline, d: sources distance
NMR: Nuclear Magnetic Resonance
MRI: Magnetic Resonance Imaging
SNR: Signal to Noise Ratio

1. Introduction

There are many reasons for using magnetic sensors in industrial and scientific applications. They are indeed contactless, accurate, easy to use, almost insensitive to temperature, moisture and dust, and cheap. The measured magnetic field depends however on many parameters, for instance the geometry of surrounding materials, their magnetic properties and so on...

It is of great interest to adjust the sensor sensitivity map, in other words the signal variation due to a small parameter variation at a given position in space, in order to optimize the sensor response for a given application.

Magnetic sensor sensitivity map can be estimated by various ap proaches. As a first example analytical approximations can be used [1], but only a limited number of simple cases can be treated that w ay. As a second example parametric numerical simulations can be made, but as the number of situations increases, at least various posi tions and orientations of a single source, the number of calculations rapidly increases as well as the time required for obtaining a result.

In nuclear magnetic resonance (NMR) the signal is often obtain ed through a pick-up coil using Faraday induction law. Recent research shows that using NMR in the range of Earth's magne tic field (50 μT) reduces the NMR linewidth achieving a high spectral resolution [5-6], magnetic field induced artifacts are smaller and it is possible to ma ke NMR measurements inside or in presence of metallic pieces [8]. H owever Earth's field NMR signal is very small due to the low nuclear spins polarization and environmental noises become very important w

hen using a conventional detecting coil [7-10]. Usually gradiometer p ick-up coils are used instead [2-4], which geometry are designed to measure the signal while reducing the noise produced by far sources.

In this paper, magnetic sensor sensitivity map is analytically cal culated for any geometry of any kind of magnetic induction sensors. Eddy currents are also taken into account. In the next section the ph ysical background of magnetic sensors is recalled. Then sensitivity map is calculated as a small local variation of permeability, conduct ivity and magnetization. In last section, sensitivity maps of various gradiometer are calculated and compared in terms of rejection powe r and measurement volume.

2. Physical background

2.1 Related Maxwell equations

Magnetic field verifies Maxwell's equations [3] and two of thes e are particularly useful for the present study:

$$\overrightarrow{\mathrm{curl}}(\vec{E}) = -\frac{\partial \vec{B}}{\partial t} \quad (1)$$

$$\overrightarrow{\mathrm{curl}}(\vec{H}) = \vec{J} \quad (2)$$

In (1), which is known as Faraday's law, $\vec{E}$ is the electric field, $\vec{B}$ is the induction field and t is time. Insofar as the electric field $\vec{E}$ is induced by the induction field $\vec{B}$ and not by electrostatic sources in the case of magnetic sensors, both electric and induction fields derive from the vector potential $\vec{A}$ as

$$\vec{E} = -\frac{\partial \vec{A}}{\partial t} \quad (3)$$

$$\vec{B} = \overrightarrow{\mathrm{curl}}(\vec{A}) \quad (4)$$

In (2), which is known as Ampere's law, $\vec{H}$ is the magnetic field and $\vec{J}$ is the current density. The induction and magnetic fields are connected together by

$$\vec{B} = \mu\vec{H} + \mu_0\vec{M} \quad (5)$$

where μ is the magnetic permeability of the material at the considered position, μ_0 the vacuum magnetic permeability and $\vec{M}$ the permanent magnetization density. Notice that induced magnetization density is taken into account in the permeability μ when it is different from μ_0. At low frequency $\vec{J}$ has two contributions: $\vec{J}_s$ which is the current density source term and $\sigma\vec{E}$ which is the induced conduction current density at the origin of eddy currents where σ is the material conductivity. Mixing all equations together, Ampere's law can be rewritten as

$$\overrightarrow{\mathrm{curl}}\left(\frac{1}{\mu}\overrightarrow{\mathrm{curl}}(\vec{A})\right) + \sigma\frac{\partial \vec{A}}{\partial t} = \vec{J}_s + \overrightarrow{\mathrm{curl}}\left(\frac{\mu_0}{\mu}\vec{M}\right) \quad (6)$$

2.2. Magnetic induction sensors

When an induction field goes through an electrical circuit $\mathcal{C}$, which path is $\mathcal{L}$ and area is $\mathcal{A}$ (Fig.1a), the voltage v appearing at the circuit terminals can be calculated using Faraday's law (1). From the first member one gets

$$\int_{\mathcal{A}} \overrightarrow{curl}(\vec{E}) \cdot d\vec{s} = \oint_{\mathrm{ABCA}} \vec{E} \cdot d\vec{l} = \int_{\mathrm{ABC}} \vec{E} \cdot d\vec{l} - v \quad (7a)$$

and from the second member one has

$$-\frac{\partial}{\partial t}\int_{\mathcal{A}} \vec{B} \cdot d\vec{s} = -\frac{\partial \varphi_s}{\partial t} \quad (7b)$$

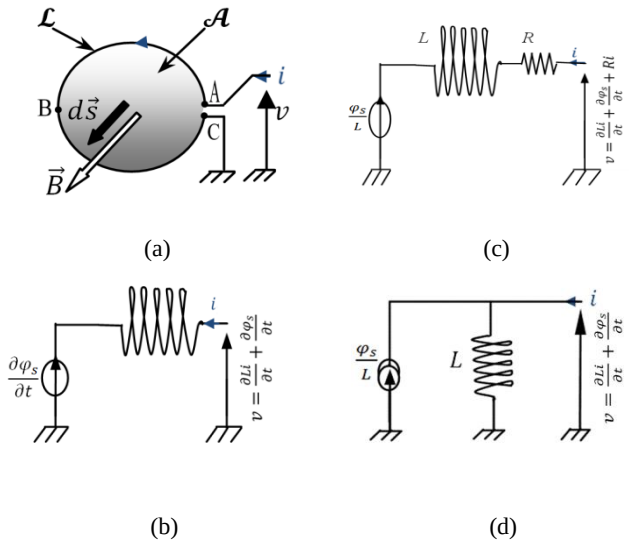

Fig.1: (a) Interaction between a magnetic field and a circuit coil. (b) Sensor equivalent circuit in the ideal case and (c) taking resistance R losses into account. (d) Thevenin-Norton transforms.

The integral over ABC in (7a) corresponds to the voltage appearing at terminals of the coil when a current i is flowing. One obtains

$$v = L\frac{\partial i}{\partial t} + \frac{\partial \varphi_s}{\partial t} \quad (8)$$

Here L is a constant known as the circuit self inductance. The voltage v, corresponds to an inductor in series with a voltage source (Fig.1b). Notice that, except in the case of superconducting materials, inductors always presents a small resistor in series due to the resistivity of the wires (Fig.1c).

Depending on the measuring conditions, the signal can be a voltage or a flux in open-circuit condition, a current in short-circuit condition, or a mix of both in intermediate condition. Using Thevenin-Norton transforms, the signal obtained in one condition can easily be changed as if it had been obtained in another condition (Fig.1d). Therefore the calculation of the sensitivity map in one condition is sufficient to deduce the one in any other conditions. We have chosen to calculate the sensitivity map in open-circuit condition in the following.

3. Sensitivity map calculation

In open-circuit condition, sensor sensitivity map S_p^{φ} is defined as the variation of the flux φ through measuring coil, as a function of the variation of a parameter p at a given position $\vec{x}$ to which the sensor is sensitive. One has

$$S_p^{\varphi} = \frac{\partial \varphi}{\partial p} \quad (9)$$

Hence for n parameters, the overall flux variation $\Delta\varphi$ can be written as the sum of integrals over space of each local parameter variation.

$$\Delta\varphi = \int S_{p1}^{\varphi}(\vec{x})\,\delta p_1(\vec{x})dv + \cdots + \int S_{p_n}^{\varphi}(\vec{x})\,\delta p_n(\vec{x})dv \qquad (10)$$

The main parameters for magnetic induction sensors are those directly insinuated in Maxwell's equations: permeability μ, conductivity σ, magnetization $\vec{M}$, current density $\vec{J}$ and geometry.

3.1. Equilibrium perturbation

Any small perturbation modifying the permeability μ by $\delta\mu$, the conductivity σ by $\delta\sigma$, the magnetization $\vec{M}$ by $\delta\vec{M}$, or the current density $\vec{J}$ by $\delta\vec{J}$, produces in turn a vector potential variation $\delta\vec{A}$ which is at the origin of the measured signal. During that perturbation, (6) becomes

$$\overrightarrow{\text{curl}}\left(\frac{\overrightarrow{\text{curl}}(\vec{A}+\delta\vec{A})}{\mu+\delta\mu}\right)+(\sigma+\delta\sigma)\frac{\partial(\vec{A}+\delta\vec{A})}{\partial t}=\vec{J_s}$$

$$+\delta\vec{J_s}+\overrightarrow{\text{curl}}\left(\frac{\mu_0(\vec{M}+\delta\vec{M})}{\mu+\delta\mu}\right) \qquad (11)$$

Assuming small variations, which is actually the case for defining sensor sensitivity, only first order terms remain and the combination of (4), (5), (6) and (11) leads to

$$\overrightarrow{\text{curl}}\left(\frac{1}{\mu}\overrightarrow{\text{curl}}(\delta\vec{A})\right)+\sigma\frac{\partial\delta\vec{A}}{\partial t}=\delta\vec{J_s}+\delta\sigma\vec{E}$$

$$+\overrightarrow{\text{curl}}\left(\frac{\delta\mu}{\mu}\vec{H}+\frac{\mu_0}{\mu}\,\delta\vec{M}\right) \qquad (12)$$

As can be seen the vector potential variation $\delta\vec{A}$ is equivalent to the vector potential that would be generated in the sensor structure by the current density $\delta\vec{J_s}+\delta\sigma\vec{E}$ and the permanent magnetization $\delta\mu\vec{H}/\mu_0+\delta\vec{M}$. That is illustrated in Fig.2.

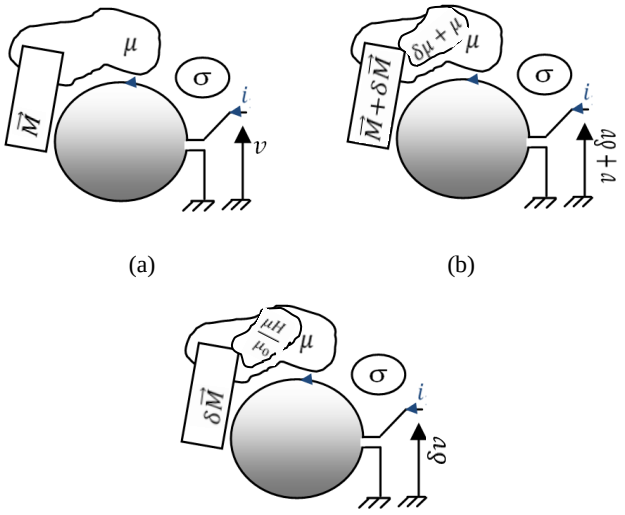

(a) (b)

c)

Fig.2: Variation of the induction field due to a perturbation. (a) Equilibrium state *before*. (b) Equilibrium state *during* the perturbation. (c) Variation between the equilibrium states *during* and *before* the perturbation.

In open-circuit condition, when the signal is a voltage or a flux variation, the current density in the measuring circuit does not vary when the perturbation occurs. Therefore there is no current flowing in the measuring circuit in the state described by (12) (Fig.2c).

3.2. General situation

The flux variation through a given circuit can be calculated with identity (13) which connects two independent equilibrium states A and B, each verifying (6). One has

$$\int \vec{J}_B\cdot\vec{A}_A\cdot dv=\int \vec{J}_A\cdot\vec{A}_B\cdot dv \qquad (13)$$

In that identity, which is similar to Gauss's Identity in electrostatics [3], the source density $\vec{J}$ includes all kinds of sources, that is to say real current densities as well as equivalent current densities deriving from permanent magnetization. The distribution of material properties should be the same in both states and when considering Eddy currents the sensor should operate in harmonic regime. In order to calculate the sensor sensitivity map, the state of equilibrium representing the variation between *during* and *before* the perturbation is chosen as state A. Therefore the vector potential is $\vec{A}_A=\delta\vec{A}$, there is no current flowing in the measuring circuit (open-circuit measuring condition) and the flux variation $\delta\varphi_m$ across the measuring circuit is the one from which the signal is derived. State A is represented in Fig.3a. The same sensor structure is chosen for state B. In that state of equilibrium however, there are no other sources than the measuring circuit carrying a current of 1A. The vector potential is $\vec{A}_B=1\,\text{A}\times\vec{\alpha}_m$. Though that state of equilibrium is used for mathematical purpose, it can be seen as a state that describes the sensor structure seen from the measuring circuit. State B is represented in Fig.3b.

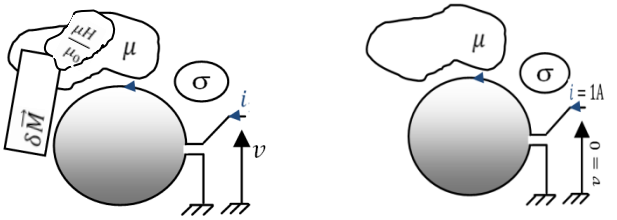

a) b)

Fig.3: States of equilibrium used for Identity (13). (a) State A represents the real situation (b) State B describes the sensor structure seen from the measuring circuit.

Using states A and B, the first member of Identity (13) is

$$\int_{\mathcal{C}_m}\vec{J}_B\cdot\delta\vec{A}_A\,dv=1\text{A}\times\oint_{\mathcal{L}_m}\delta\vec{A}\cdot d\vec{l}=1\text{A}\times\delta\varphi_m \qquad (14)$$

where the volume of the integral reduces to the volume of the measuring circuit $\mathcal{C}_m$ since in state B there is only a current in this circuit. The volume of the measuring circuit can be conveniently seen as a path $\mathcal{L}_m$ and a cross section. As to the second member of Identity (13), one has directly

$$1\text{A}\times\int\vec{J}_A\cdot\vec{\alpha}_m\,dv=1\text{A}\times\int\left(\delta\vec{J_s}+\delta\sigma\vec{E}\right)\cdot\vec{\alpha}_m\,dv$$

$$+1\mathrm{A}\times\int\overrightarrow{\mathrm{curl}}\left(\frac{\delta\mu}{\mu}\vec{H}+\frac{\mu_0}{\mu}\,\delta\vec{M}\right)\cdot\vec{\alpha}_m\,dv \qquad (15)$$

Consequently one finds from the Identity (13) that the flux variation $\delta\varphi_m$ in the measuring circuit after the integration by parts of the last term of (15) is

$$\delta\varphi_m=\int\left(\delta\vec{J}_s+\delta\sigma\vec{E}\right)\cdot\vec{\alpha}_m\,dv+\int\left(\frac{\delta\mu}{\mu}\vec{H}+\frac{\mu_0}{\mu}\,\delta\vec{M}\right)\wedge\vec{\alpha}_m ds$$

$$+\int\left(\frac{\delta\mu}{\mu}\vec{H}+\frac{\mu_0}{\mu}\,\delta\vec{M}\right)\cdot\vec{\beta}_m\,dv \qquad (16)$$

where $\vec{\beta}_m=\overrightarrow{\mathrm{curl}}(\vec{\alpha}_m)$, $\vec{\alpha}_m$ and $\vec{\beta}_m$ are respectively the vector potential and the induction field that would be generated in the sensor structure by the measuring circuit $\mathcal{C}_m$ when carrying 1 A. They can be seen as a kind of sensor environment description seen from the measuring circuit. The surface integral in (16) tends to zero since there are no sources at infinity and $\vec{H}\wedge\vec{\alpha}_m$ decreases at least as $1/r^5$ whereas the surface of integration increases only as r^2. It stays finally

$$\delta\varphi_m=\int\left(\delta\vec{J}_s+\delta\sigma\vec{E}\right)\cdot\vec{\alpha}_m\,dv+\int\left(\frac{\delta\mu}{\mu}\vec{H}+\frac{\mu_0}{\mu}\,\delta\vec{M}\right)\cdot\vec{\beta}_m\,dv \quad (17)$$

Current density variations $\delta\vec{J}_s$ depends on current variation δi_j in a given circuit $\mathcal{C}_j$. With $\delta\vec{J}_s=\delta\vec{J}_j$ by definition one has

$$\delta\varphi_m=\int_{\mathcal{C}_j}\delta\vec{J}_j\cdot\vec{\alpha}_m\,dv=\delta i_j\int_{\mathcal{A}_j}\vec{\beta}_m\cdot d\vec{s}=L_{mj}\,\delta i_j \qquad (18)$$

L_{mj} represents the induction tensor which diagonal coefficients are the self inductances and cross coefficients are the mutual inductances. $\mathcal{A}_j$ is any area bounded by the circuit path $\mathcal{L}_j$. The flux variation $\delta\varphi_m$ in the measuring $\mathcal{C}_m$ induced by a permeability variation $\delta\mu$, a conductivity variation $\delta\sigma$ or a magnetization variation $\delta\vec{M}$ is finally

$$\delta\varphi_m=\int\frac{\delta\mu}{\mu}\,\vec{H}\cdot\vec{\beta}_m\,dv+\int\delta\sigma\vec{E}\cdot\vec{\alpha}_m\,dv$$

$$+\int\frac{\mu_0}{\mu}\,\delta\vec{M}\cdot\vec{\beta}_m\,dv\;+L_{mj}\,\delta i_j \qquad (19)$$

4. Application

4.1 Low field NMR

Nuclear magnetic resonance (NMR) is used to investigate the molecular structure in the presence of an applied magnetic field which yields a proportional proton precession frequency [7]. Because the NMR frequency is sensitive to the local magnetic field, it is an excellent probe for direct measurement of the interaction between nucleus (proton) and their magnetic field environment. Conventional NMR experiments are based on Faraday detector resonant circuit [2]. The sample precessing magnetization induces a voltage v in the detector which scales as B^2 making the signal to noise ratio (SNR) increasing along with magnetic field strength [7]. However increasing magnetic field strength results in a complicated and much expensive system, it also contributes to arise spatial variation in magnetic susceptibility by creating local gradient, limiting the spatial resolution [3]. An alternative approach is to detect NMR signals at low magnetic fields (<10 mT) by using more sensitive sensors [11], because the induced sample polarization is very small at this field range [4]. The high magnetic field sensitivity of DC SQUID offers the possibility to measure the low resulting NMR signal [11]. The DC SQUID combines the macroscopic quantum phenomena of Josephson effect and the flux quantization [2]; it is based on a small superconducting loop, broken by two Josephson junctions, which detect changes in magnetic flux rather than rate of flux changes [11]. The output voltage is a periodic function of the applied magnetic flux, with a quantum flux period φ_0, equal to $2.07\text{x}10^{-15}$ Wb. The magnetic field to measure is introduced by a superconducting input coil coupled to the SQUID via a mutual inductance, as shown in Fig.4a. Therefore changing current in the input coil induces a flux change detected by the SQUID which is in turn, converted to output voltage by using a feedback circuit, called flux locked loop as shown in Fig.4b [5-11]. The SQUID and input coil are housed in a superconductor material and connected to an output pick-up coil to form an extremely low noise magnetometer, see Fig.4a. The superconducting pick-up coil forms a flux transformer with the SQUID input coil.

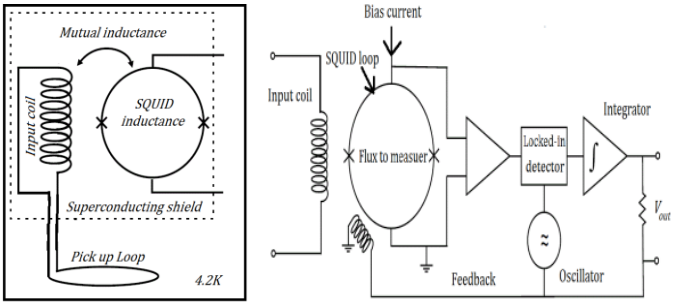

(a) (b)

Fig.4: DC SQUID. (a) Schematic of a DC SQUID coupled to a pick-up loop. (b) DC SQUID electronic with feedback.

4.2 Low field MRI

As seen in section 4.1 the precession frequency of the nuclear spins is proportional to the local magnetic field. By controlling the local strength of the magnetic field with an applied field gradients, it's possible to determine the spatial distribution of the nuclear spins from the measured signal. Magnetic Resonance Imaging (MRI) is therefore able to image the human body noninvasively. As in low field NMR it is advantageous to reduce magnetic field strength, by using highly sensitive sensor such as a DC SQUID. Low field MRI reduces system cost and offers an open geometry [11], susceptibility artifacts are reduced [8-11] and proton contrast T_1 is increased between cells [9], it also makes possible the imaging in presence of metallic pieces and imaged-guided biopsy with metallic needles [8]. However at low field signal is in the range of few kilohertz and below while environmental noise and RF interference are important. These noises contribute to reduce SNR when the SQUID is coupled to conventional detection coil, like a simple loop (Fig.4a). As a solution gradiometers pick-up coils are used instead of simple loops. Gradiometers reduce distant noise sources efficiently

ensuring an important shielding for environmental electromagnetic interference and Nyquist noise from tissue deep in the sample and room temperature imaging coil [2-10].

5. Pick-up coil design and sensitivity map

Different pick-up coil geometries used in SQUID applications are compared efficiency. Sensitivity map for all cases is treated numerically. Inductances of different pick-up coils are close to input coil inductance usually used in SQUID application ($\approx 1\mu H$). Indeed, inductance matching ensures the maximum sensitivity for a given pick-up coil area [11]. All pick-up coils calculated hereafter are 20 mm diameter and are wounded with 1 mm diameter wire.

Simple loop pick-up coil provides a good signal but it is also sensitive to different environmental noise. The slow decrease of the axial response to magnetic field in $1/x^3$ contributes to inductively couple unwanted noise to the receiver and affects substantially the SNR. This kind of coil could be used only in shielded rooms. In Fig.5b, we show the variation of the simple coil sensitivity field $\vec{\beta}_m$. Values are given in μT/A. This coil has an inductance of 1.024μH.

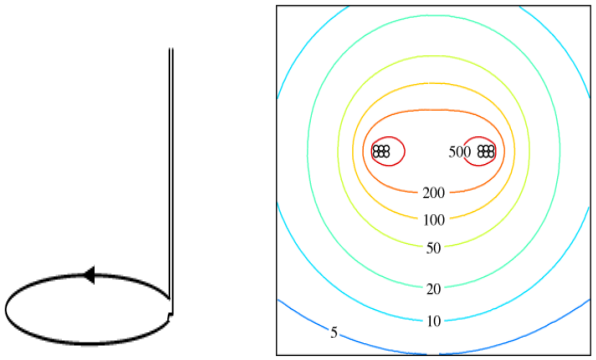

(a) (b)

Fig 5: (a) Simple loop design. (b) Corresponding sensitivity map for a coil of 6 turns.

Gradiometer pick-up coils offer the possibility to collect signal without important RF shielding. Fig.6a shows a first order axial gradiometer composed of two simple loops wounded in opposite direction about the same axis and separated by a baseline distance *b*.

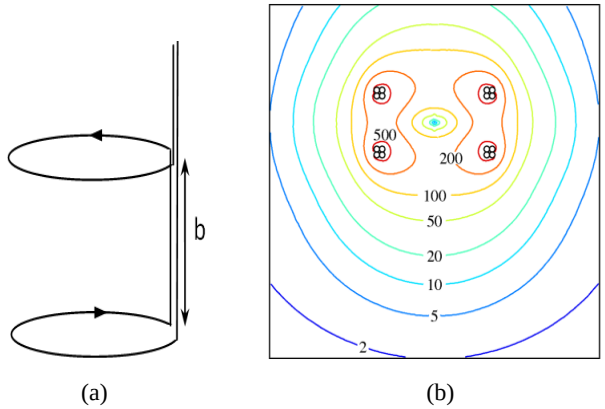

(a) (b)

Fig.6: (a) First order axial gradiometer.(b) Corresponding sensitivity map with 4 turns in each loop.

At small distances magnetic source is well measured by the nearest loop, whereas at large distances gradiometers acts as derivative operator of first order $\partial B/\partial x$ in axial direction increasing noise canceling. The slope of rejection varies as $1/x^4$ as shown in Fig.6b, yielding a better shielding than simple loop. However the measurement volume corresponding to maximum sensitivity is achieved when $d \leq b$ and noise sources still inductively coupled. This axial gradiometer has an inductance of $0.842\ \mu$H.

Second order axial gradiometer is the most used gradiometer in N MR and MRI low field. As shown in Fig.7a, it is wounded as $+1-2+1$ turn. The axial variation of the magnetic field is in $1/x^5$, which offers better rejection to magnetic field noise than two later pic k-up coils. Nevertheless, the source to measure must be closer than its baseline *b*, which is hardly achievable when pick-up loop is used in cryogenic environment. The measurement has 3dB losses because the lower loop has less turns (Fig.7b). This axial gradiometer has an inductance of $1.269\ \mu$H.

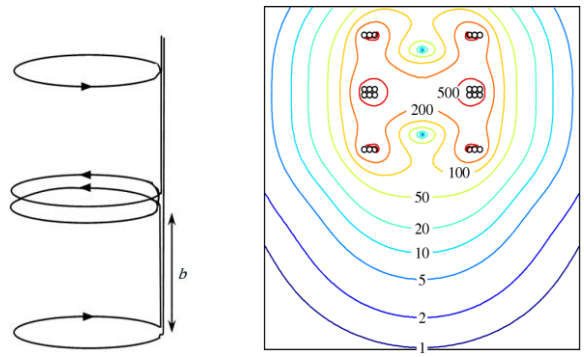

(a) (b)

Fig.7: (a) Second order gradiometer design. (b) Corresponding sensitivity map with 3-turn outer loops and 6-turn center loop.

Radial gradiometer wounded as shown in Fig.8a is of great interest. It combines the surface optimum sensitivity of simple loop (Fig.6b) while decreasing drastically magnetic noises from far sources as shown in Fig.8b. It shows also a better uniformity of volume sensing for closer position, in axial and radial direction. Therefore gradiometric flux transformer coupled with a planar gradiometer pick-up coil will be able to provide an optimal coupling between the external desired magnetic field sources and the SQUID's input coil, achieving a higher SNR. The inductance of radial gradiometer of Fig.8b is $1.005\ \mu$H.

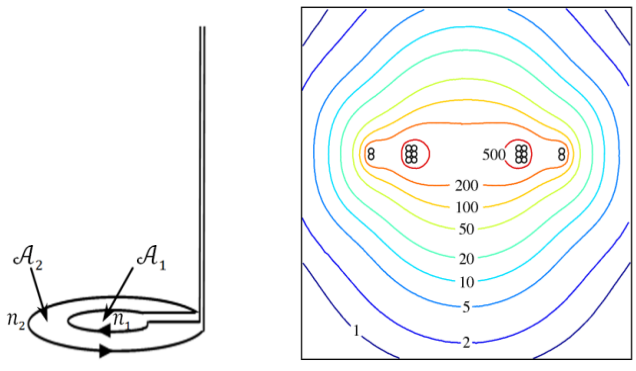

(a) (b)

Fig.8: (a) Radial gradiometer design. (b) Corresponding sensitivity map with number of turns $n_1 = 6$ and $n_2 = 2$, satisfying the relation: $\mathcal{A}_1 n_1 = \mathcal{A}_2 n_2$, when the outer radius is $\sqrt{3}$ larger than inner radius.

5.1 Comparison and analyze

All pick-up coils mentioned above were designed to have similar inductance in order to match SQUID input coil and also to ensure a relevant comparison according to their size. However, since one has integer number of turns, inductance values are not strictly the same. Therefore, sensitivity map of first order gradiometer is under estimated compared to sample loop and radial gradiometer, whereas second order gradiometer sensitivity map is over estimated. At 10 mm and below the pick-up coils measured magnetic field is $\vec{\beta}_m = 200\,\mu\mathrm{T/A}$ for the simple loop coil, less than $100\,\mu\mathrm{T/A}$ for gradiometer of first order, $50\,\mu\mathrm{T/A}$ for the second order gradiometer and $100\,\mu\mathrm{T/A}$ for the radial gradiometer. It can be concluded that simple loop has a better sensitivity than the radial and first order gradiometer while the second order gradiometer has the lowest sensitivity. For a complete comparison however it is necessary to study the rejection power of far spurious magnetic sources.

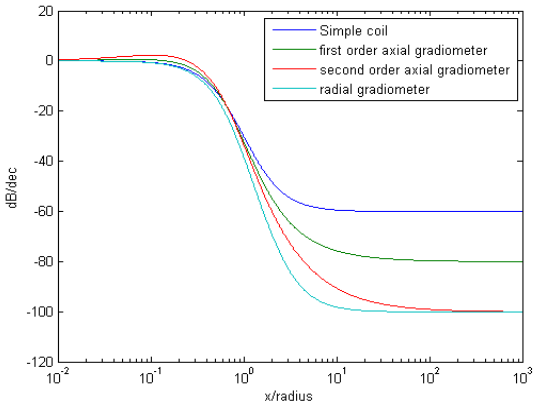

Fig.9: Sensitivity is given in logarithmic scale dB\dec as a function of axial distance divided by coil radius.

Fig.9 shows the slope or the decreasing sensitivity as the function of the axial distance. It can be observed that closer sources are well measure up to the coil radius and then decrease by 60 dB/dec for the simple coil, 80 dB/dec for first order gradiometer and 100 dB/dec for radial and second order gradiometers. Taking into account local sensitivity and far source rejection, the radial gradiometer offers the best compromise.

6. Conclusion

A theoretical approach has been studied and demonstrated analytically in order to illustrate local variation of sensitivity map for a given sensor. Indeed, the identity equation's, simplify greatly the estimation of physical material parameters commonly involved in magnetic field measuring applications. It can integrate any variation in the sensor environment such as variation in conductivity, magnetic permeability, current sources and magnetization.

Analytical approach performed by numerical simulations contributes to have a relevant sight on different sensor coil performances used for instance in low field NMR and MRI. We have introduced a new design consisting of radial gradiometer with higher performances of rejection power than those usually used. The use of this geometry can for instance greatly improve the patient access in MR Imaging and reach a higher SNR according to minimized distance due to its planar geometry.

References

1. A. Gonzalez-Nakazawa, W. Yang, K. Hennessey. "An analytical approach for modelling electro-magnetic tomography sensor", Sensor Review, Vol. 28 Iss: 3.
2. R Mcdermott. 2004. "SQUID-detected Magnetic Resonance Imaging in Microtesla Magnetic Fields".
3. P. Poincelot. Précis d'électromagnétisme théorique. Dunod, 1963.
4. W. Myers, D Slichter. "Calculated signal-to-noise ratio of MRI detected with SQUIDs and Faraday detectors in fields from 10 μT to 1.5 T". Journal of Magnetic Resonance Volume 186, Issue 2, June 2007, Pages 182-192.
5. R. McDermott, A.H Trabesinger, M.Muck, E.L. Hahn, Alex Pines, and John Clarke, Sciences 295, 2247 (2002).
6. R.Macdermott. "Microtesla MRI with Superconducting Qauntum Interference Device".
7. Ya. S. Greenberg. "Application of superconducting quantum interference devices to nuclear magnetic resonance". Rev. Mod. Phys. 70, 175–222 (1998).
8. M. Mößle. S. Han. "SQUID-detected microtesla MRI in the presence of metal Michael".
9. S. Lee, M Möβle. "SQUID-Detected MRI at 132 μT with T1 contrast weighted at 10 μT-300 mT".
10. Seton HC Hutchison JMS, Bussell DM. Meas Sci Techno l. "Gradiometer pick-up coil design for a low field SQUID-MRI system". 1999.
11. J. Clarke, A. I. Braginski (Eds.) The SQUID Handbook. Vol. I and II.